Active damping for acoustic levitation in air

Bos, Vincent; Wesselingh, Jasper; Verbiest, Gerard J.; Steeneken, Peter G.

DOI
10.1063/5.0210800

Publication date
2024

Document Version
Final published version

Published in
AIP Advances

RESEARCH ARTICLE | SEPTEMBER 05 2024

Active damping for acoustic levitation in air

Vincent Bos ; Jasper Wesselingh; Gerard J. Verbiest ; Peter G. Steeneken

AIP Advances 14, 095009 (2024)
https://doi.org/10.1063/5.0210800

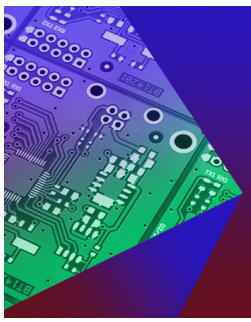

Active damping for acoustic levitation in air

Cite as: AIP Advances 14, 095009 (2024); doi: 10.1063/5.0210800
Submitted: 12 July 2024 • Accepted: 13 August 2024 •
Published Online: 5 September 2024

Vincent Bos,[1,a)] Jasper Wesselingh,[2] Gerard J. Verbiest,[1] and Peter G. Steeneken[1]

AFFILIATIONS

[1] Faculty of Mechanical Engineering, Delft University of Technology, Mekelweg 2, 2628 CD Delft, The Netherlands
[2] ITEC B.V., Jonkerbosplein 52, 6534 AB Nijmegen, The Netherlands

[a)] Author to whom correspondence should be addressed: v.bos@tudelft.nl

ABSTRACT

Acoustic levitation is an attractive and versatile technique that offers several advantages in terms of particle size, range, reconfigurability, and ease of use with respect to alternative levitating techniques. In this paper, we study the use of active damping to improve the response time and positioning precision of an acoustic levitator operating in air. We use a laser Doppler vibrometer to measure the velocity of a levitated particle. Using this information, a control algorithm is designed and implemented to provide active damping. By system identification and modeling, we demonstrate that the active damper mechanism is well-predictable by models and can be electronically reconfigured and controlled.

I. INTRODUCTION

During the past decades, the interest in acoustic fields for the levitation of particles in air has been steadily growing.[1] Its ability to levitate virtually any material,[2,3] including solids, liquids, and living samples, makes acoustic levitation an attractive and versatile technique that offers several advantages in terms of particle size, range, reconfigurability, and ease of use with respect to alternative levitation methods,[4] such as magnetic[5] and optical levitation.[6,7] By equipping ultrasound transducer arrays with fast electronic control, it became possible to levitate and move multiple particles simultaneously while also controlling their orientation.[8] This enables a wide range of applications for acoustic levitation in chemistry,[9,10] biophysics,[11] 3D displays,[12] and microassembly.[2,13]

A major challenge in controlling a particle by acoustic fields, instead of using contact forces, is the relatively small stiffness and damping force in the field-generated acoustic levitation traps. As a consequence, noise and disturbances that act on a levitating particle will excite underdamped oscillations[14] with long relaxation times. Although increasing the stiffness of the field is beneficial, it is limited by the maximum acoustic power of the ultrasound transducers and results in high electrical power usage and thus heat generation. The relatively low stiffness of the acoustic field causes low fundamental resonance frequencies f_n of the levitating particles, which, in combination with the low air damping,[15] lead to high quality factors $(Q \approx \frac{1}{2\zeta})$ of a few hundred and result in long decay times $\tau = \frac{Q}{\pi f_n}$ in the order of seconds. Vibrations induced by disturbances or trap movement thus persist for a long time, diminishing the precision and speed by which acoustic levitating particles can be moved and positioned. Increasing the gas damping force in acoustic levitation is not desired, since it requires operating in high-pressure chambers with specialized gases. Moreover, increased gas damping would limit the maximum speed by which particles can be moved. Therefore, alternative methods to increase the damping and reduce the relaxation time of acoustically levitating particles are needed.

Since passive methods for increasing damping of acoustically levitated objects are not easily implementable, it is of interest to investigate the feasibility of using active damping for stabilizing acoustic levitating particles. Active damping requires a feedback loop that monitors particle motion with a sensor and generates a feedback signal to alter the acoustic field.

For position sensing, high-speed cameras provide detailed information at a high time resolution. However, the particle position data are only available after image processing, which is computationally expensive and thus usually performed after the recording is made.[16,17] For the implementation of feedback, the particle velocity has to be measured in real-time, so offline data processing is not possible. Therefore, the conventional high-speed camera setup as used by Jiang *et al.*[17] or Andrade *et al.*[16] cannot be employed. In contrast, a laser Doppler vibrometer (LDV) can measure the velocity of a surface and output the data in real-time and can even be used for (sub-)millimeter-sized particles. For example, Argo *et al.*[18] showed how to measure the vibrations of an air bubble of 1 mm in water and Koyama *et al.*[19] applied the same concept to measure the posi-

tion of a 0.1 mm particle using an LDV. In addition, Andrade *et al.*[16] showed how to measure the acoustic field pressure itself using an LDV.

For high bandwidth feedback, it is important to use a dedicated computing unit for the acoustic levitator. Beasley *et al.*[20] showed how to use a system-on-module (SOM) to generate the transducer signals for the acoustic field, and to perform real-time data acquisition. They also showed how to generate square wave signals using the field-programmable gate array (FPGA) on the SOM. In this way, the transducer signals can be controlled individually at a high time resolution, achieving a phase resolution of $\pi/125$ rad.[17] This is in contrast to the widely used Arduinos that have a typical phase resolution of just $\pi/12$ rad.[3] In addition, as the FPGA has a very high time resolution, pulse-width modulated (PWM) signals can be generated as described by Sun.[21] In this way, the acoustic field contains less undesired features, as the PWM signals can be converted into nearly ideal sinusoidal signals.

To design a controller that performs active damping on the levitated particle, it is required to know the dynamics of the complete system. This involves the dynamics of the levitated particle, the sensor, and the computing unit, as well as delays present in the loop. Identification of the dynamics of an acoustically levitated particle has been reported several times. Jiang *et al.*[17] showed how a transfer function model can be estimated. The trap is moved using a chirp signal, and the particle response is captured using a high-speed camera. The amplitude of the vibration spectrum is fit to the transfer function model, yielding the stiffness of the acoustic field. However, their methodology does not provide any timing information. In addition, Perez *et al.*[14] showed how the damping coefficient can be estimated from the step response of an acoustically levitated particle, using a camera. So, although some aspects of system identification of a levitated particle have been demonstrated, the complete identification has not.

In this paper, we realize active damping by combining an LDV with an FPGA-controlled acoustic levitator. We use active damping to improve the response time and positioning precision of an acoustic levitator. To implement feedback, we measure the particle velocity using a laser Doppler vibrometer. Using a computing unit with real-time data acquisition (Zynq PicoZed), we analyze the vibrometer signal and compute the new trap position to damp the particle motion. In order to design a stable and optimal feedback controller, we first perform system identification. This implies that we identify the complete system dynamics of a levitated particle in the frequency domain. We also determine the phase response, which is crucial for the design of a feedback controller.

Finally, we show that the active damping provided by the feedback controller can decrease the quality factor from $Q = 440$ down to $Q = 0.6$, close to the optimal critically damped case $Q = 0.5$. Active damping can thus be used to increase the speed and precision by which levitating particles can be controlled.

II. METHOD

In this section, we describe the acoustic levitator setup, the laser Doppler vibrometer (LDV), and the data processing and feedback implementation used for active damping.

A. Acoustic levitation setup

The acoustic levitator consists of two opposing arrays of 64 Murata MA40S4S piezoelectric ultrasound transducers (PUTs) [see Fig. 1(a)]. Each PUT has a diameter of 1 cm, and each transducer array has a rectangular layout of 8 by 8 cm, as shown in Fig. 1(b). As Fig. 1(c) shows, the distance between the transducer arrays is 9 cm and we levitate a spherical polyethylene (PE) particle with a diameter of 1.1 mm.

An acoustic trap (a point with a large acoustic trapping force, at which the particle levitates) is formed using electronic phase focusing.[3,17] This implies that the phase offset of each individual transducer is chosen such that the resulting acoustic field is focused at the trap location, while the amplitude of all transducer signals is kept the same,

$$\theta_i^{\text{focus}} = \tau_i \omega_t = \frac{r_i - r_f}{\lambda} \cdot 2\pi. \tag{1}$$

Here, θ_i is the phase offset of transducer i, ω_t equals the angular frequency of the transmitted acoustic signal, τ_i equals the sound wave travel time from transducer position r_i to focus point r_f, and λ equals the wavelength of the acoustic signal.

The trap is located in the middle of the levitator by setting an additional phase difference of 180° between the bottom and top transducer arrays (a z-trap). This results in a trap that has a high vertical acoustic radiation force such that gravity can be overcome. The resulting individual phase offset of each transducer, therefore, consists of a focusing component and a trap-signature component ($\theta_i^{\text{tot}} = \theta_i^{\text{focus}} + \theta_i^{\text{trap}}$), as explained by Marzo *et al.*[8] The pressure, measured with a calibrated microphone (Bruel and Kjaer, type 1708) near the trap, was found to be 2.8 kPa. By varying the phase shifts of the top and bottom arrays, the trap position can be controlled in the vertical direction.

In short, 128 pulse-width modulated (PWM) voltage signals are generated using an FPGA-based Zynq PicoZed 7015 system-on-module (SOM) to create the acoustic levitation trap. Analog filters are used to convert the PWM signals to sinusoidal signals of 39.8 kHz, which is near the resonance frequency of the ultrasound transducers. 128 power amplifiers (PAs) are used to amplify the sinusoidal signals to a peak-to-peak amplitude of 28.6 V and individually drive the Murata ultrasound transducers. In Sec. S4 of the supplementary material, some further details are presented about the transducer signal generation.

Figure 1(d) shows a schematic illustration of the actuation scheme and measurement setup. We use a high-speed camera (HSC) in combination with a telecentric lens focused on the levitated particle to record the motion of the particle at 200 f/s (fps). Afterward, we determine the particle position for each frame using the imfindcircles algorithm in MATLAB.

B. Feedback implementation

To implement feedback, we use a laser Doppler vibrometer (LDV, Polytec OVF-534), which points at the particle through a hole in the upper transducer array and measures the velocity of the levitating particle as shown in Fig. 2(a). The measurement distance (the distance from the particle to the front of the lens) is 209 mm, and the spot size is 28 μm. The LDV converts the measured z-component of

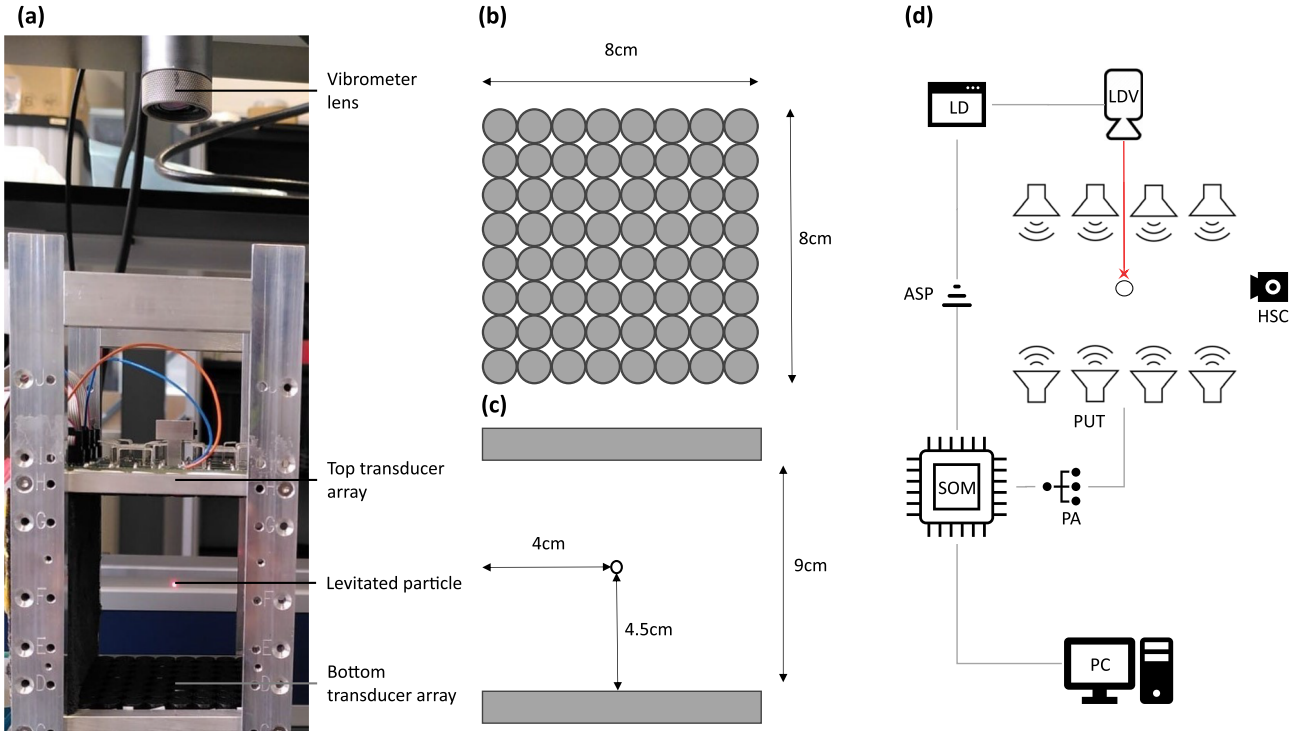

FIG. 1. (a) Photo of the acoustic levitator. (b) Top view of the transducer array. (c) Side view of the transducer array. (d) Setup schematic. SOM: system-on-module, PA: power amplifier, PUTs: piezoelectric ultrasonic transducers, LDV: laser Doppler vibrometer, LD: laser decoder, ASP: analog signal processing, and HSC: high-speed camera.

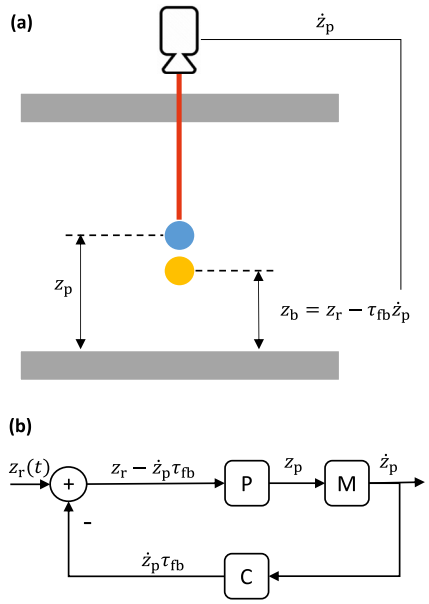

FIG. 2. Feedback implementation. (a) Trap position for feedback; z_p: particle position, z_b: trap position, z_r: reference position, and τ_{fb}: feedback gain. (b) Block diagram feedback concept; C: controller, P: plant [levitated particle, defined in Eq. (4)], and M: velocity sensor (LDV).

the particle velocity to an analog voltage signal. A low-pass filter with a cutoff frequency $f_c = 600$ Hz is used to remove high-frequency noise. The filtered signal is provided to the analog-to-digital converter (ADC), which has a sampling rate of 800 kHz. After the data acquisition, the signal is digitally high-pass filtered to remove low-frequency noise ($f_c = 4$ Hz) and drift. We exert a feedback force on the levitated particle by setting the acoustic trap position z_b at a different point as the actual particle position z_p, as shown in Fig. 2(a) and Fig. S1 of the supplementary material.

To implement active damping to the particle, the trap position z_b is calculated based on the motion of the particle according to

$$z_b = z_r - \tau_{fb}\dot{z}_p. \tag{2}$$

Here, we multiply the measured velocity of the levitated particle $\dot{z}_p$ by the gain τ_{fb} and subtract this from the reference setpoint value z_r. This reference value z_r is the location where we aim to stabilize the particle and can be a function of time t.

To assess the effect of feedback on the levitated particle's motion, the particle is modeled as a simple mass–spring damper system (see also Sec. S1 of the supplementary material), with particle mass m, acoustic field stiffness k, and damping coefficient c,

$$m\ddot{z}_p + c\dot{z}_p + k(z_p - z_r + \tau_{fb}\dot{z}_p) = 0. \tag{3}$$

Note that Eq. (2) is used to calculate the acoustic force $-k(z_p - z_b)$ on the particle in the presence of feedback. This equation can be mass normalized using the natural frequency $\omega_n^2 = k/m$ as follows:

$$\ddot{z}_p + 2\zeta\omega_n\dot{z}_p + \omega_n^2(z_p - z_r) = 0, \tag{4}$$

where ζ denotes the damping ratio, which is the sum of air-drag (ζ_d) and feedback (ζ_{fb}) damping ($\zeta = \zeta_d + \zeta_{fb}$). The damping ratio ζ is directly related to the quality factor using $Q = \frac{1}{2\zeta}$, and the natural frequency is related to the eigenfrequency using $\omega_n = 2\pi f_n$. The damping force yielded from the feedback loop yields the following damping ratio:

$$\zeta_{fb} = \frac{1}{2}\tau_{fb}\omega_n. \tag{5}$$

The Stokes drag force acting on an oscillating sphere in laminar flow can be estimated according to Ref. 22 and leads to the following damping ratio:

$$\zeta_d = \frac{9}{4}\frac{\mu}{\omega_n\rho_p R^2}\left(1 + \frac{R}{\delta}\right), \tag{6}$$

where δ denotes the penetration depth according to

$$\delta = \sqrt{\frac{2\mu}{\rho_0\omega}}, \tag{7}$$

where μ is the fluid viscosity, ω is the frequency of oscillation, ρ_p is the particle density, and ρ_0 is the fluid density.

If the particle is displaced by a distance $\Delta z_{p,0}$, the settling time T_s is defined[23] as the time needed before the oscillations are faded out to 5% of the step amplitude $\Delta z_{p,0}$,

$$T_s \equiv -\ln(0.05)\frac{1}{\zeta\omega_n} = -\ln(0.05)\frac{2Q}{\omega_n}. \tag{8}$$

The value of ζ_d is typically 1.3×10^{-3} for a polyethylene particle with a radius of 1.1 mm and a resonance frequency of 44 Hz, which results in an estimated Q-factor of $Q = 3.8 \times 10^2$ (see Table I) and a typical settling time of $T_s = 8$ s. This long settling time is a clear motivation for implementing active damping to increase ζ and decrease the settling time T_s.

TABLE I. Open-loop system identification: characteristic dynamic quantities of the levitated particle (air drag damped). Used parameter values: temperature $T = 298$ K, pressure $p_0 = 101$ kPa, viscosity $\mu = 1.85 \times 10^{-5}$ Pa s, air density $\rho_0 = 1.2$ kg m^{-3}, particle density $\rho_p = 1.0 \times 10^3$ kg m^{-3}, and particle radius $R = 0.55$ mm.

Parameter	Value	Source	Source description
Q	4.4×10^2	Figure 3	Step response
Q	1.2×10^2	Figure 4	Bode diagram
Q	3.8×10^2	Equation (6)	Stokes drag for vibrations
f_n	4.4×10^1 Hz	Figure 3	Step response
τ_d	0.7 ms	Figure 4	Bode diagram

III. RESULTS

In this section, we first analyze the open-loop dynamics of the system to identify the system parameters Q and ω_n. Then, we analyze the closed-loop dynamics of the system shown in Fig. 2 to determine the system parameters as a function of the feedback gain τ_{fb}.

We perform open-loop system identification by moving the reference setpoint $z_r(t)$ while monitoring the resulting particle motion. In the first identification method, we toggle the setpoint between two positions to generate a step response. We monitor the particle motion using the high-speed camera, which provides us a measurement of the particle position $z_p(t)$ as a function of time t [see Fig. 5(b)]. We then determine the eigenfrequency f_n from the

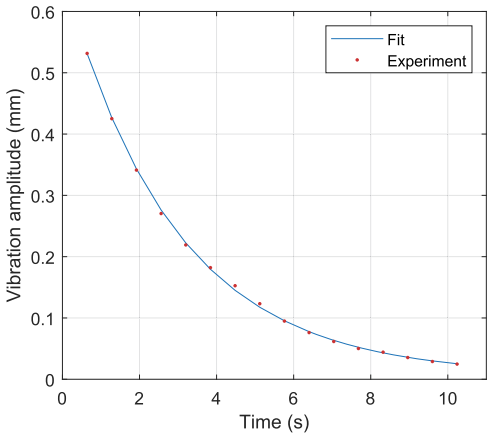

FIG. 3. Identification of the open-loop system using the step response: vibration amplitude of the levitated particle after a step in trap position [as shown in Fig. 5(b)]. Data are fit to the model defined in Eq. (4), yielding the following parameter values: $Q = 4.4 \times 10^2$ and $f_n = 4.4 \times 10^1$ Hz.

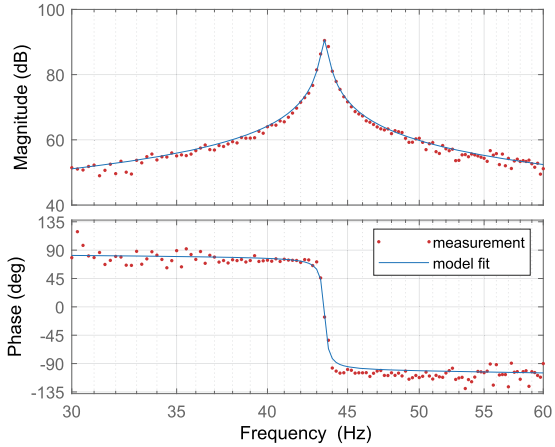

FIG. 4. Identification of the open-loop system using the frequency response: The Bode diagram shows the output-over-input ratio $H \equiv \frac{\dot{z}_p}{z_r}$. The data are fit to Eq. (10). This yields fit values $f_n = 4.4 \times 10^1$ Hz, $Q = 1.2 \times 10^2$, and $\tau_d = 0.7$ ms. The magnitude axis is expressed in dB: $20\log_{10}|H|$.

discrete Fourier transform (DFT) of $z_p(t)$ (see the supplementary material, Fig. S8). The amount of damping is found by fitting the amplitude decay profile at the eigenfrequency of the DFT-transformed data as shown in Figs. 3 and 5(b). In the supplementary material, Sec. S3.1, more details of the data processing are presented.

For the second identification method, we monitor the particle dynamics with the LDV while exciting it with a multisine reference signal $z_r(t)$. The multisine signal used as a reference signal $z_r(t)$ contains all frequencies from 0.25 to 80 Hz with a resolution of 0.25 Hz and is constructed according to the following equation, where the parameters are listed in the supplementary material, Table S2:

$$z_r(t) = \sum_{i=1}^{N} A \sin(\omega_i t + \varphi_i). \tag{9}$$

As the LDV velocity signal $\dot{z}_p$ and the setpoint signal $z_r(t)$ are both synchronously recorded by the SOM, we can calculate the frequency response. This is shown in the Bode diagram in Fig. 4. We fit both the amplitude and phase of the measured response $\left(\frac{\dot{z}_p}{z_r}\right)$ to the following equation:

$$H(s) = \mathcal{L}\left\{\frac{\dot{z}_p(t)}{z_r(t)}\right\} = \frac{s \cdot \omega_n^2}{s^2 + 2\zeta\omega_n s + \omega_n^2} \cdot e^{-\tau_d s}. \tag{10}$$

Equation (10) corresponds to Eq. (4), as is derived in the supplementary material, Sec. S1.3, but has an extra time delay τ_d included. The time delay is needed in the model to account for delays that are present in the levitator and measurement hardware. The controller (SOM) causes the main part of the total delay. The origin of the delay is further investigated in the supplementary material, Table S1, by taking a closer look at the individual hardware components. The phase response shown in Fig. 4 remains abundantly within the range from −180 to +180°, which guarantees stability when applying negative feedback.[24] We note that the phase shift due to the delay at resonance is relatively small, $\omega_n\tau_d = 2\pi \times 0.03$ rad, such that it is a reasonable approximation to neglect it in Eq. (4).

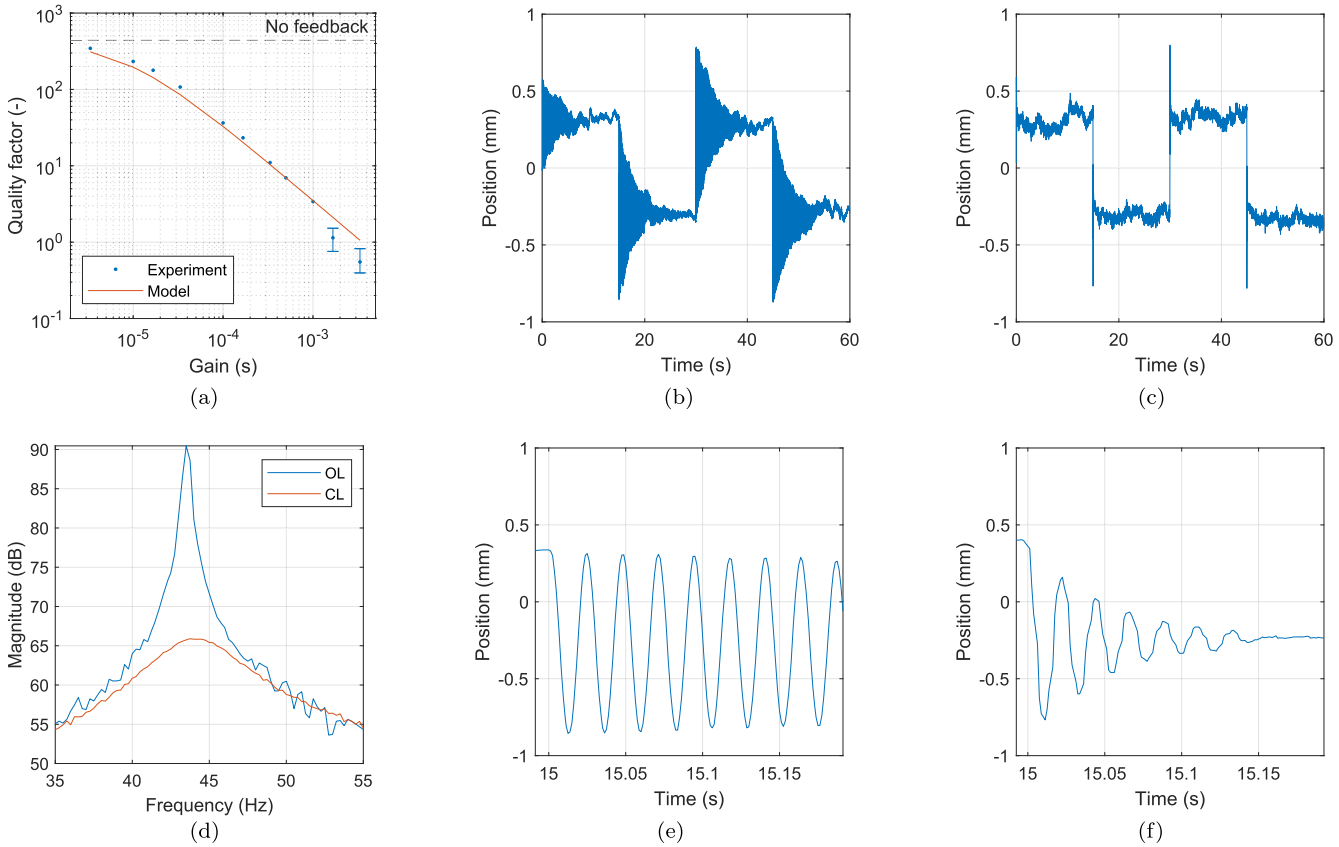

FIG. 5. Performance of the closed-loop system. (a) Quality factor Q for increasing gain level τ_{fb}. The amplitude decay of each step response is fit to Eq. (4). The red line is calculated using Eq. (2): $Q = 1/\tau_{fb}\omega_n$. (b) Particle response (z_p) to a square wave reference signal $z_r(t)$. No feedback was applied ($\tau_{fb} = 0$). (c) Particle response (z_p) to a square wave reference signal $z_r(t)$. In this case, feedback was applied ($\tau_{fb} = 0.5$ ms). (d) Bode diagram using a multisine reference signal (as Fig. 4). The data are fit using the model defined in Eq. (10), $H \equiv \frac{\dot{z}_p}{z_r}$. Fit values: open loop (OL): $Q = 1.24 \times 10^2$ and closed loop (CL) ($\tau_{fb} = 0.5$ ms): $Q = 7.4$. Magnitude in dB: $20\log_{10}|H|$. (e) Zoom-in of panel (b); settling time $T_s = 9.7$ s. (f) Zoom-in of panel (c); settling time $T_s = 0.16$ s.

TABLE II. Feedback performance, observed in the step response.

τ_{fb} (ms)	$Q(-)$	T_s (s)	Source
0	4.4×10^2	9.7×10^2	Figure 3
0.50	7.4	1.6×10^{-1}	Figures 5(a) and 5(c)
3.3	6×10^{-1}	1×10^{-2}	Figure 5(a)

Table I gives an overview of the model parameter values found from open-loop system identification.

To quantify the amount of damping added by the feedback loop described in Fig. 2(b), we perform system identification on the closed-loop system. First, the step response is analyzed for a range of different feedback gain values τ_{fb}, as shown in Figs. 5(a)–5(c). In this experiment, the gain is increased and the Q factor at each gain value is determined by fitting the step response, as in Fig. 3. The gain is increased until the particle starts to show unstable vibrations for $\tau_{fb} > 3.3$ ms. The highest damping observed here corresponds to a Q-factor of 0.6, which is close to critical damping $Q_{critical} = 0.5$. The instability at higher gains is attributed to horizontal vibrations of the particle and is further investigated in the supplementary material, Secs. S2.2–S2.4. Based on this investigation, the optimal gain value is chosen as the gain at which the LDV feedback induced noise equals the noise level in the absence of feedback, at $\tau_{fb} = 0.50$ ms. At this gain value, a Q-factor of 7.4 was measured and the Bode diagram for a multisine reference signal is plotted in Fig. 5(d) and compared to the open-loop response. For both datasets, the response was fit to Eq. (10).

To demonstrate the improvement in response time by implementation of active damping, the particle is moved using a square-wave reference signal $z_r(t)$. This signal is a simple example of position indexing (start–stop movement), which directly shows why it is so beneficial to have active damping. Figure 5(b) shows the particle position for a square wave reference signal $z_r(t)$, when no feedback on the particle is present ($\tau_{fb} = 0$). The long period of almost 10 seconds over which the particle remains vibrating clearly reveals the low damping ratio $\zeta_d = 0.0011$ and high quality factor $Q = 440$. Figure 5(e) gives a closer look at the particle response near the time at which the setpoint z_b is moved. As expected of a highly undamped system, the particle vibrates for a time of the order of the settling time $T_s = 9.7$ s (see Table II). Figure 5(c) shows the particle position for the same square wave reference signal $z_r(t)$, while feedback is present. Clearly, the particle is able to track the reference signal much faster. After the setpoint moves, the particle settles at the new setpoint value within $T_s = 0.16$ s. Figure 5(f) zooms in on the step response, and Table II provides an overview of the performance increase by the implementation of active damping.

IV. DISCUSSION

We have demonstrated in Fig. 5(a) that active damping can substantially reduce the effective quality factor of an acoustic levitated particle by a factor of more than 700. The damping coefficient depends on the feedback gain and closely follows Eq. (2) with Q-factor $Q = \frac{1}{2\zeta}$, as can be seen by comparing experimental and model points in Fig. 5(a).

Air drag damping predicted by Stokes' drag theory in Eq. (6) is about 16% higher than the measured damping coefficient (Table I). The lower experimental damping coefficient may be related to deviations from the laminar flow assumption that underlies the theory or the assumed parameter values (such as fluid density and viscosity).

The Q-factor measured from the Bode diagram in Fig. 4 is about three times lower than the one measured in the step response (Table I). This might be related to the multisine approach for measuring Q, in comparison with the ringdown method. When actuating the particle simultaneously with many different frequencies, it might be difficult to stay in the linear regime, especially when Q is high. Potentially nonlinear effects could broaden the resonance peak. We expect these effects to play less of a role at lower Q values. Other effects that might affect Q are the frequency resolution, frequency stability, and drift of the setup. Based on this, we only use the step response Q-factors for the analysis.

Active damping comes at the cost of additional induced noise. This can be seen in Fig. 5(c), where the particle shows noisy vibrations during a constant setpoint reference signal z_r. There are two causes for those vibrations: First, the signal coming from the vibrometer contains noise. This noise source is amplified by the feedback gain and added to the setpoint signal. For this reason, an analog low-pass filter was implemented [Fig. 1(d), analog signal processing (ASP)], which partly reduced this effect. The effect of LDV noise is further investigated in the supplementary material, Sec. S2.3. Employing methods to reduce the noise level of the LDV sensor might reduce the undesired particle vibrations and related instabilities at high gain.

Second, the cross-sensitivity of the LDV for vibration modes along different axes can bring in additional feedback noise and can even destabilize the system. For a laser beam reflected from a sphere, the movement of the sphere in the x and y directions will also cause a change in the distance between the sphere surface and the LDV. Therefore, besides z-axis motion, motion in the x and y axes will also be detected by the LDV and can be excited by moving the setpoint $z_r(t)$.[25] If the feedback loop for these off-axis directions is positive, it can cause instability as soon as the loop gain becomes larger than one. This is shown in the supplementary material, Fig. S4, where the resonance corresponding to horizontal movement is located around 14 Hz. Using a sensor that is only sensitive to the desired particle movement direction would improve stability. This could be accomplished, for example, by using another means of sensing, such as acoustic echoing (as proposed by Ref. 20), or by using multiple LDVs to monitor the particle's 3D motion.

V. CONCLUSION

In this work, we show that using a vibrometer and a SOM, the dynamics of an acoustically levitated particle can be identified. Using this information, a control algorithm was designed and implemented using an LDV for fast feedback to provide active damping. From Fig. 5, it becomes clear that active damping can add a significant amount of damping to a levitated particle. Active damping can be effective and is orders of magnitude larger, up to a factor 700, than damping provided by air drag. We showed that this enables reducing the particle's Q nearly down to the critically damped case ($Q = 0.6$), which is also reflected by the settling time, which was

reduced from 9.7 s to about 0.01 s. This is in contrast to earlier attempts[20] that, using acoustic echoing, were able to detect the particle position but did not demonstrate feedback. By system identification and modeling, we demonstrated that the active damping mechanism is well-predictable by models and can be electronically reconfigured and controlled, as shown by the fit in Fig. 5(a). We note that the presented feedback method is not limited to acoustic levitation but might also be implemented for other levitating systems. Ultimately, we anticipate that active damping as introduced here might become a key technique for rapid particle manipulation using acoustic levitation fields.

SUPPLEMENTARY MATERIAL

The supplementary material elaborates in more detail on the findings presented in this paper. It contains among others details about the setup, step-by-step derivations of the presented equations, and additional experimental findings.

ACKNOWLEDGMENTS

This work was financed by ITEC B.V. and co-financed by the Netherlands Enterprise Agency (RVO).

AUTHOR DECLARATIONS

Conflict of Interest

The authors have no conflicts to disclose.

Author Contributions

Vincent Bos: Conceptualization (equal); Data curation (equal); Formal analysis (equal); Investigation (equal); Methodology (equal); Validation (equal); Visualization (equal); Writing – original draft (equal). **Jasper Wesselingh**: Conceptualization (equal); Methodology (equal); Resources (equal); Software (equal); Supervision (equal). **Gerard J. Verbiest**: Conceptualization (equal); Supervision (equal); Writing – review & editing (equal). **Peter G. Steeneken**: Conceptualization (equal); Funding acquisition (equal); Supervision (equal); Writing – review & editing (equal).

DATA AVAILABILITY

The data that support the findings of this study are available from the corresponding author upon reasonable request.

REFERENCES

[1] M. A. B. Andrade, N. Pérez, and J. C. Adamowski, "Review of progress in acoustic levitation," Braz. J. Phys. **48**(2), 190–213 (2018).
[2] V. Vandaele, A. Delchambre, and P. Lambert, "Acoustic wave levitation: Handling of components," J. Appl. Phys. **109**(12), 124901 (2011).
[3] A. Marzo, A. Barnes, and B. W. Drinkwater, "TinyLev: A multi-emitter single-axis acoustic levitator," Rev. Sci. Instrum. **88**(8), 085105 (2017).
[4] E. H. Brandt, "Levitation in physics," Science **243**(4889), 349–355 (1989).
[5] M. D. Simon and A. K. Geim, "Diamagnetic levitation: Flying frogs and floating magnets (invited)," J. Appl. Phys. **87**(9), 6200–6204 (2000).
[6] A. Ashkin and J. M. Dziedzic, "Optical levitation of liquid drops by radiation pressure," Science **187**(4181), 1073–1075 (1975).
[7] A. Ashkin and J. M. Dziedzic, "Optical levitation by radiation pressure," Appl. Phys. Lett. **19**(8), 283–285 (1971).
[8] A. Marzo, S. A. Seah, B. W. Drinkwater, D. R. Sahoo, B. Long, and S. Subramanian, "Holographic acoustic elements for manipulation of levitated objects," Nat. Commun. **6**(1), 8661 (2015).
[9] F. Priego-Capote and L. de Castro, "Ultrasound-assisted levitation: Lab-on-a-drop," TrAC, Trends Anal. Chem. **25**(9), 856–867 (2006).
[10] S. Santesson and S. Nilsson, "Airborne chemistry: Acoustic levitation in chemical analysis," Anal. Bioanal. Chem. **378**(7), 1704–1709 (2004).
[11] A. Scheeline and R. L. Behrens, "Potential of levitated drops to serve as microreactors for biophysical measurements," Biophys. Chem. **165-166**, 1–12 (2012).
[12] T. Fushimi, A. Marzo, B. W. Drinkwater, and T. L. Hill, "Acoustophoretic volumetric displays using a fast-moving levitated particle," Appl. Phys. Lett. **115**(6), 064101 (2019).
[13] V. Vandaele, P. Lambert, and A. Delchambre, "Non-contact handling in microassembly: Acoustical levitation," Precis. Eng. **29**(4), 491–505 (2005).
[14] N. Pérez, M. A. B. Andrade, R. Canetti, and J. C. Adamowski, "Experimental determination of the dynamics of an acoustically levitated sphere," J. Appl. Phys. **116**(18), 184903 (2014).
[15] S. Tsujino, Y. Sato, Y. Takeda, and T. Tomizaki, "Oscillation resonances and anisotropic damping of the motion of acoustically levitated droplets in single-axis acoustic levitators," Appl. Phys. Lett. **115**(5), 053702 (2019).
[16] M. A. B. Andrade, N. Pérez, and J. C. Adamowski, "Experimental study of the oscillation of spheres in an acoustic levitator," J. Acoust. Soc. Am. **136**(4), 1518–1529 (2014).
[17] L. Jiang, Y. Wang, S. Fan, X. Yu, and X. Li, "Transfer function modeling and dynamic performance analysis of single-axis acoustic-levitation systems," Mechatronics **92**, 102984 (2023).
[18] T. F. Argo IV, P. S. Wilson, and V. Palan, "Measurement of the resonance frequency of single bubbles using a laser Doppler vibrometer," J. Acoust. Soc. Am. **123**(6), EL121–EL125 (2008).
[19] D. Koyama, H. Kotera, N. Kitazawa, K. Yoshida, K. Nakamura, and Y. Watanabe, "Vibration of a single microcapsule with a hard plastic shell in an acoustic standing wave field," IEEE Trans. Ultrason. Ferroelectrics Freq. Control **58**(4), 737–743 (2011).
[20] W. Beasley, B. Gatusch, D. Connolly-Taylor, C. Teng, A. Marzo, and J. Nunez-Yanez, "Ultrasonic levitation with software-defined FPGAs and electronically phased arrays," in *2019 NASA/ESA Conference on Adaptive Hardware and Systems (AHS)* (IEEE, 2019), pp. 41–48.
[21] J. Sun, "Pulse-width modulation," in *Dynamics and Control of Switched Electronic Systems: Advanced Perspectives for Modeling, Simulation and Control of Power Converters*, edited by F. Vasca and L. Iannelli (Springer, London, 2012), pp. 25–61.
[22] V. K. Gupta, G. Shanker, and N. K. Sharma, "Experiment on fluid drag and viscosity with an oscillating sphere," Am. J. Phys. **54**, 619–622 (1986).
[23] S. S. Rao, *Mechanical Vibrations*, 5th ed. (Pearson Education South Asia Pte Ltd., 2011).
[24] G. F. Franklin, J. David Powell, and A. Emami-Naeini, *Feedback Control of Dynamic Systems*, 6th ed. (Pearson Education, 2010), International Edition.
[25] N. Sugita, T. Oshino, and T. Shinshi, "Nonlinear coupling between radial and axial vibrations during single-axis acoustic levitation in mid-air," Int. J. Mech. Sci. **246**, 108159 (2023).